

SID



سرویس های ویژه



سرویس ترجمه تخصصی



کارگاه های آموزشی



بلاگ مرکز اطلاعات علمی



عضویت در خبرنامه

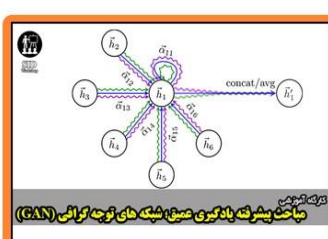


فیلم های آموزشی

کارگاه های آموزشی مرکز اطلاعات علمی جهاد دانشگاهی



کارگاه آنلاین آشنایی با پایگاه های اطلاعات علمی بین المللی و ترند های جستجو



مباحث پیشرفته یادگیری عمیق؛ شبکه های توجه گرافی (Graph Attention Networks)



کارگاه آنلاین مقاله نویسی IEEE و ISI ویژه فنی و مهندسی



MHD Unsteady Flow and Heat Transfer of Micropolar Fluid through Porous Channel with Expanding or Contracting Walls

Y. Asia, A. Kashif and A. Muhammad[†]

Centre for Advanced Studies in Pure and Applied Mathematics, Bahauddin Zakariya University, Pakistan

[†]Corresponding Author Email: mashraf_mul@yahoo.com

(Received March 26, 2014; accepted September 6, 2015)

ABSTRACT

The unsteady laminar incompressible flow and heat transfer characteristics of an electrically conducting micropolar fluid in a porous channel with expanding or contracting walls is investigated. The relevant partial differential equations have been reduced to ordinary ones. The reduced system of ordinary differential equations (ODEs) has been solved numerically by lower-upper (LU) triangular factorization or Gaussian elimination and successive over relaxation (SOR) method. The effects of some physical parameters such as magnetic parameter, micropolar parameters, wall expansion ratio, permeability Reynolds number and Prandtl number on the velocity, microrotation, temperature and the shear and couple stresses are discussed.

Keywords: Magnetohydrodynamics (MHD); Expanding or contracting walls; Porous channel; Wall expansion ratio; Quasi-linearization.

1. INTRODUCTION

There are many fluids which are important from the industrial point of view, and display non-Newtonian behavior. Due to the complexity of such fluids, several models have been proposed but the micropolar model has been found to be the most appropriate one. It has been experimentally predicted that the fluids which could not be characterized by Newtonian relationships, indicated significant reduction in shear stress near a rigid body. The micropolar model has been successful in explaining such behaviors of the non-Newtonian fluids. Since its introduction, the micropolar fluid has been a hot area of research, and therefore many investigators have studied the related flow and heat transfer problems in different geometries. For example, natural convection heat transfer between two differentially heated concentric isothermal spheres utilizing micropolar fluid has been numerically investigated by Khoshab and Dehghan, (2011). Govardhan and Kishan (2011) studied the MHD effects on the unsteady boundary layer flow of an incompressible micropolar fluid over a stretching sheet when the sheet was stretched in its own plane. Ashmawy (2014) considered the problem of fully developed natural convective micropolar fluid flow in a vertical channel, under the slip boundary conditions for fluid velocity. The effect of the presence of a thin perfectly conductive baffle on the fully developed laminar mixed convection in a vertical channel containing

micropolar fluid was analyzed by Umavathi (2011).

There has been a growing interest of the research community in flows through porous channel with expanding or contracting walls. This is due to their significance in many biological and engineering models, including the transport of biological fluids through contracting or expanding vessels, the synchronous pulsation of porous diaphragms, the air circulation in the respiratory system, and the regression of the burning surface in solid rocket motors. Due to their extensive applications, many studies related to the internal flows in different geometries with contracting or expanding domains have been carried out. Xin-Hue *et al.* (2011) investigated the flow of a viscoelastic fluid in porous channels with expanding or contracting walls. Analytic solution of the problem was obtained by employing the homotopy analysis method (HAM) to the nonlinear ODEs arising due to the introduction of similarity transformation. The study was further extended to the micropolar fluids by Xin-Hue *et al.* (2010). Xinhui *et al.* 2012 considered the asymmetric viscoelastic fluid in a rectangular domain bounded by two porous moving channels with expanding or contracting walls.

To our best knowledge, no researcher has yet considered the thermal behavior of micropolar fluid flow in a porous channel with expanding or contracting walls. Therefore, in this paper, we consider the characteristics of an unsteady, laminar, incompressible, and electrically conducting

micropolar fluid in a channel having permeable expanding or contracting walls, with an external magnetic field acting normally. A similarity transformation has been employed to construct a set of nonlinear coupled ordinary differential equations in the dimensionless form, which are numerically solved by employing an algorithm based on the Quasi-linearization and finite difference discretization. The ease in obtaining the numerical solution using the technique makes it superior than the shooting like approach used in our earlier investigations (for example, Ali *et al.* 2014)

2. PROBLEM FORMULATION

We consider the flow and heat transfer characteristics of an unsteady, incompressible, viscous and electrically conducting micropolar fluid in a porous channel with expanding or contracting walls under the action of an external magnetic field. Compared to the imposed field, the induced magnetic field is assumed to be negligible. Further, the magnetic Reynolds number (defined as the ratio of the product of characteristic length and fluid velocity, to the magnetic diffusivity) is assumed to be small. For small magnetic Reynolds number, the magnetic field will tend to relax towards a purely diffusive state. Moreover, it is assumed that there is no applied polarization voltage which implies the absence of any electric field. Otherwise, the electrical current flowing in the fluid will give rise to an induced magnetic field which would exist if the fluid was an electrical insulator. But, in the present study, we have taken the fluid to be electrically conducting. The distance between the porous walls is $2a(t)$, which is much smaller than the width and length of the channel. Both the channel walls have the same permeability and are expanding or contracting uniformly at a time-dependent rate $\dot{a}(t)$.

The geometry of the problem suggests that the Cartesian coordinate system may be chosen with the origin at the middle of the channel, as shown in the Fig. 1. With u and v being the velocity components in, respectively, the x and y directions, the governing equations for the problem in the absence of body couples are:

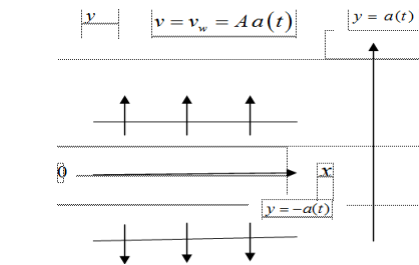


Fig. 1. Physical model of the problem.

$$\frac{\partial u}{\partial x} + \frac{\partial v}{\partial y} = 0, \tag{1}$$

$$\frac{\partial u}{\partial t} + u \frac{\partial u}{\partial x} + v \frac{\partial u}{\partial y} = -\frac{1}{\rho} \frac{\partial p}{\partial x} + \left(\frac{\mu + \kappa}{\rho} \right) \left(\frac{\partial^2 u}{\partial x^2} + \frac{\partial^2 u}{\partial y^2} \right) + \frac{\kappa}{\rho} \frac{\partial N}{\partial y} - \frac{\sigma_e B_0^2}{\rho} u, \tag{2}$$

$$\frac{\partial v}{\partial t} + u \frac{\partial v}{\partial x} + v \frac{\partial v}{\partial y} = -\frac{1}{\rho} \frac{\partial p}{\partial y} + \left(\frac{\mu + \kappa}{\rho} \right) \left(\frac{\partial^2 v}{\partial x^2} + \frac{\partial^2 v}{\partial y^2} \right) - \frac{\kappa}{\rho} \frac{\partial N}{\partial x}, \tag{3}$$

$$\rho j \left(\frac{\partial N}{\partial t} + u \frac{\partial N}{\partial x} + v \frac{\partial N}{\partial y} \right) = -\kappa \left(2N + \frac{\partial u}{\partial y} - \frac{\partial v}{\partial x} \right) + \gamma \left(\frac{\partial^2 N}{\partial y^2} + \frac{\partial^2 N}{\partial x^2} \right), \tag{4}$$

$$\rho c_p \left(\frac{\partial T}{\partial t} + u \frac{\partial T}{\partial x} + v \frac{\partial T}{\partial y} \right) = k_0 \left(\frac{\partial^2 T}{\partial x^2} + \frac{\partial^2 T}{\partial y^2} \right) + \sigma_e B_0^2 u^2, \tag{5}$$

Here, μ , ρ , T , c_p and k_0 are, respectively, the dynamic viscosity, density, temperature, specific heat at constant pressure, and thermal conductivity of the fluid. Further, the symbols j , γ and κ denote the microinertia per unit mass, the spin gradient viscosity and the vortex viscosity of micropolar fluids. Finally, σ_e is the electrical conductivity of the fluid, B_0 is the strength of the external magnetic field, and N is the component of the microrotation normal to the xy -plane.

It is important to mention that Eq. (1) is the continuity equation, Eqs. (2) and (3) correspond to the x - and y -components of the momentum equation (respectively), Eq. (4) is the microrotation equation, and finally Eq. (5) is the heat equation.

The micro-inertia density is the intensity of the inertial forces due to the micro particles of the fluid, whereas the microrotation is defined as the rotation of microscopic particles of a fluid, and is evaluated by taking the curl of the velocity field at microscopic level.

We also assume that there is strong concentration of microelements and the microelements close to the walls are unable to rotate. This assumption leads to the following boundary conditions for the problem:

$$\left. \begin{aligned} u(x, -a) = 0, v(x, -a) = -A\dot{a}, N(x, -a) = 0, \\ T(x, -a) = T_1, u(x, a) = 0, v(x, a) = A\dot{a}, \\ N(x, a) = 0, T(x, a) = T_2. \end{aligned} \right\} \tag{6}$$

Here A is the measure of the wall permeability, and the dots denote the derivative w. r. t. the time t , whereas T_1 and T_2 (with $T_1 > T_2$) are the fixed temperatures of the lower and upper channel walls respectively.

We introduce the following similarity transformations:

$$\left. \begin{aligned} \eta &= \frac{y}{a(t)}, u = -\nu a^{-2} x F_{\eta}(\eta, t), \\ v &= \nu a^{-1} F(\eta, t), N = \nu a^{-3} x G(\eta, t), \\ \theta &= \frac{T - T_2}{T_1 - T_2}. \end{aligned} \right\} \quad (7)$$

It is to note that, with the above mentioned transformation, Eq. (1) is identically satisfied which means that the proposed velocity field is compatible with the continuity equation. It may, therefore, represent the possible fluid motion.

After eliminating the pressure term from the governing equations, we use Eq. (7) in the resulting equations, and arrive at:

$$\left. \begin{aligned} (1 + \frac{\kappa}{\mu}) F_{\eta\eta\eta\eta} - \frac{\kappa}{\mu} G_{\eta\eta} + \alpha(3F_{\eta\eta} + \eta F_{\eta\eta\eta}) + \\ (F_{\eta} F_{\eta\eta} - F F_{\eta\eta\eta}) - \nu^{-1} a^2 F_{\eta\eta} - \\ \frac{a^2 \sigma_e B_0^2}{\mu} F_{\eta\eta} = 0, \end{aligned} \right\} \quad (8)$$

$$\left. \begin{aligned} \frac{\gamma}{j\mu} G_{\eta\eta} + \alpha(3G + \eta G_{\eta}) + (F_{\eta} G - F G_{\eta}) \\ - \frac{\kappa a^2}{\mu j} (2G - F_{\eta\eta}) - \nu^{-1} a^2 G_t = 0, \end{aligned} \right\} \quad (9)$$

$$\theta_{\eta\eta} - \text{Pr}(F - \eta\alpha)\theta_{\eta} - \frac{\rho c_p}{k_0} a^2 \theta_t = 0. \quad (10)$$

Here, $\alpha = \frac{a \dot{a}(t)}{\nu}$ is the wall expansion ratio,

$\text{Re} = \frac{Aa\dot{a}}{\nu}$ is the permeability Reynolds number,

and $\text{Pr} = \frac{\mu c_p}{k_0}$ is the Prandtl number.

The boundary conditions acquire the form:

$$\left. \begin{aligned} \eta = -1; F = -\text{Re}, F_{\eta} = 0, G = 0, \theta = 1, \\ \eta = 1; F = \text{Re}, F_{\eta} = 0, G = 0, \theta = 0. \end{aligned} \right\} \quad (11)$$

Finally, we set $f = \frac{F}{\text{Re}}$, $g = \frac{G}{\text{Re}}$, and consider the

case following Majdalani and Zhou, 2003 when

α is a constant, $f = f(\eta)$, $g = g(\eta)$ and $\theta = \theta(\eta)$,

which leads to $\theta_t = 0$, $g_t = 0$ and $f_{\eta\eta t} = 0$.

Thus we have the following equations

$$\begin{aligned} (1 + C_1) f_{\eta\eta\eta\eta} - C_1 g_{\eta\eta} + \alpha(3f_{\eta\eta} + \eta f_{\eta\eta\eta}) \\ + \text{Re}(f_{\eta} f_{\eta\eta} - f f_{\eta\eta\eta}) - M f_{\eta\eta} = 0, \end{aligned} \quad (12)$$

$$C_3 g_{\eta\eta} + \alpha C_2 (3g + \eta g_{\eta}) + \quad (13)$$

$$C_2 \text{Re}(f_{\eta} g - f g_{\eta}) - C_1 (2g - f_{\eta\eta}) = 0,$$

$$\theta_{\eta\eta} - \text{Pr}(\text{Re} f - \eta\alpha)\theta_{\eta} = 0, \quad (14)$$

where $M = \frac{a^2 B_0^2 \sigma_e}{\mu}$ is magnetic parameter,

$C_1 = \frac{\kappa}{\mu}$ is vortex viscosity parameter, $C_2 = \frac{j}{a^2}$ is

microinertia density parameter and $C_3 = \frac{\gamma}{\mu a^2}$ is

spin gradient viscosity parameter.

The boundary conditions (11) are reduced as

$$\left. \begin{aligned} \eta = -1; f = -1, f_{\eta} = 0, g = 0, \theta = 1 \text{ and} \\ \eta = 1; f = 1, f_{\eta} = 0, g = 0, \theta = 0. \end{aligned} \right\} \quad (15)$$

3. NUMERICAL SOLUTION

We use quasi-linearization to construct three sequences of vectors $\{f^{(k)}\}$, $\{g^{(k)}\}$ and $\{\theta^{(k)}\}$,

which converge to the numerical solutions of Eqs. (12), (13) and (14) respectively. To construct

$\{f^{(k)}\}$ we linearize Eq. (12), by retaining only the first order terms, as follows:

We set

$$\begin{aligned} \phi(f, f_{\eta}, f_{\eta\eta}, f_{\eta\eta\eta}, f_{\eta\eta\eta\eta}) \equiv (1 + C_1) f_{\eta\eta\eta\eta} \\ + \alpha(3f_{\eta\eta} + \eta f_{\eta\eta\eta}) + \text{Re}(f_{\eta} f_{\eta\eta} - f f_{\eta\eta\eta}) - C_1 g_{\eta\eta} - M f_{\eta\eta} \\ + \phi(f^{(k)}, f_{\eta}^{(k)}, f_{\eta\eta}^{(k)}, f_{\eta\eta\eta}^{(k)}, f_{\eta\eta\eta\eta}^{(k)}) + \\ (f^{(k+1)} - f^{(k)}) \frac{\partial \phi}{\partial f^{(k)}} + (f_{\eta}^{(k+1)} - f_{\eta}^{(k)}) \frac{\partial \phi}{\partial f_{\eta}^{(k)}} \\ + (f_{\eta\eta}^{(k+1)} - f_{\eta\eta}^{(k)}) \frac{\partial \phi}{\partial f_{\eta\eta}^{(k)}} + (f_{\eta\eta\eta}^{(k+1)} - f_{\eta\eta\eta}^{(k)}) \frac{\partial \phi}{\partial f_{\eta\eta\eta}^{(k)}} \\ + (f_{\eta\eta\eta\eta}^{(k+1)} - f_{\eta\eta\eta\eta}^{(k)}) \frac{\partial \phi}{\partial f_{\eta\eta\eta\eta}^{(k)}} = 0, \end{aligned} \quad (16)$$

which yields

$$\begin{aligned} (1 + C_1) f_{\eta\eta\eta\eta}^{(k+1)} + (\eta\alpha - \text{Re} f^{(k)}) f_{\eta\eta\eta}^{(k+1)} \\ + (3\alpha + \text{Re} f_{\eta}^{(k)} - M) f_{\eta\eta}^{(k+1)} + \\ (\text{Re} f_{\eta\eta}^{(k)}) f_{\eta}^{(k+1)} - \text{Re} f_{\eta\eta\eta}^{(k)} f^{(k+1)} \\ = -\text{Re} f_{\eta\eta\eta}^{(k)} f^{(k)} + C_1 g_{\eta\eta}^{(k)} + \text{Re} f_{\eta}^{(k)} f_{\eta\eta}^{(k)} \end{aligned} \quad (17)$$

Now Eq. (17) gives a system of linear differential equations, with $f^{(k)}$ being the numerical solution vector of the k^{th} equation. To solve the linear ODEs, we replace the derivatives with their central difference approximations, giving rise to the

sequence $\{f^{(k)}\}$, generated by the following linear system:

$$Bf^{(k+1)} = C \tag{18}$$

with $B \equiv B_{n \times n}(f^{(k)})$ and $C \equiv C_{n \times 1}(f^{(k)})$, where n is the number of grid points. On the other hand, Eqs. (13) and (14) are linear in g and θ respectively, and therefore, in order to generate the sequences $\{g^{(k)}\}$ and $\{\theta^{(k)}\}$, we write:

$$C_3 g_{\eta\eta}^{(k+1)} + \alpha C_2 (3g^{(k+1)} + \eta g_{\eta}^{(k+1)}) + C_1 (f_{\eta\eta}^{(k+1)} - 2g^{(k+1)}) + C_2 \text{Re} (f_{\eta}^{(k+1)} g^{(k+1)} - f^{(k+1)} g_{\eta}^{(k+1)}) = 0, \tag{19}$$

$$\theta_{\eta\eta}^{(k+1)} - \text{Pr} (\text{Re} f^{(k+1)} - \eta \alpha) \theta_{\eta}^{(k+1)} = 0, \tag{20}$$

Importantly $f^{(k+1)}$ is considered to be known in the above equations and its derivatives are approximated by the respective central differences approximations.

It is important to note that the coefficient matrix B in Eq. (18) will be pentadiagonal and not diagonally dominant, and hence the iterative method like Successive over relaxation (SOR) may fail or work very poorly. Therefore, some direct method like Lower-Upper (LU) triangular factorization or Gaussian elimination with full pivoting (to ensure stability) may be employed. On the other hand, Eqs. (19) and (20) will give rise to the diagonally dominant algebraic system when discretized using the central differences, which allows us to use the SOR method. Lastly, we may also improve the order of accuracy of the solution by using polynomial extrapolation scheme.

4. RESULTS AND DISCUSSION

In this section, we will interpret the graphical and tabular presentation of our results. The physical quantities of our interest are the shear stresses, the couple stresses and the heat transfer rates at the channel walls which are, respectively, proportional to $f''(-1), g'(-1)$ and $\theta'(-1)$.

Because of the symmetry of the problem, the results are given only at the lower wall. The physical parameters of the problem are the Reynolds number Re , the magnetic parameter M , the Prandtl number Pr , the wall expansion ratio α and the micropolar parameters C_1, C_2 and C_3 . We shall study the effect of the parameters on $f''(-1), g'(-1)$ and $\theta'(-1)$, as well as, on the velocity profiles $f(\eta), f'(\eta)$, the

microrotation profile $g(\eta)$, and the heat profile $\theta(\eta)$. It is to note that $\alpha < 0$ or $\alpha > 0$ according to the case when the channel walls are contracting or expanding, whereas $\text{Re} > 0$ for suction.

The values of micropolar parameters C_1, C_2 & C_3 are chosen arbitrarily (given in Table 1), whereas the first case corresponds to the Newtonian fluid.

Table 1 Values of micropolar parameters used in the present study

Cases	C_1	C_2	C_3
1	0	0	0
2	2	0.4	0.3
3	4	0.8	0.4
4	6	1.2	0.5
5	8	1.6	0.6

Table 2 shows the convergence of our numerical results as the step-size decreases, which gives us confidence on our computational procedure.

Table 2 Dimensionless velocity $f(\eta)$ on three grid sizes and extrapolated values for $C_1 = 4, C_2 = 0.8, C_3 = 0.4, \text{Re} = 5, M = 4, \alpha = 2.5$ and $\text{Pr} = 1.5$

η	$f(\eta)$			
	1 st grid ($h=0.02$)	2 nd grid ($h=0.01$)	3 rd grid ($h=0.005$)	Extrapolated values
0.2	0.4439	0.4435	0.4435	0.4434
0.4	0.7927	0.7921	0.7919	0.7919
0.6	0.9860	0.9854	0.9852	0.9852
0.8	1.0259	1.0255	1.0255	1.0254
1.0	1	1	1	1

Table 3 shows that the effect of micropolar structure of the fluid is to reduce the shear stresses while increasing the couple stresses and the heat transfer rates at the channel walls, whether the walls are expanding or contracting. It is further noted that, compared with the shear and couple stresses, the effect of the micropolar parameters on the heat transfer rate is not much pronounced. It is perhaps due the reason that the micropolar parameters do not appear in the heat equation (please see Eq. (14)), and therefore do not influence the heat transfer rate directly.

Table 3 Effect of the micropolar parameters on $f''(-1), g'(-1)$ and $\theta'(-1)$ for $\text{Re}=1, M=4$ and $\text{Pr}=1.5$

Cases	$\alpha = -1.5$		
	$f''(-1)$	$g'(-1)$	$\theta'(-1)$
1	4.8919	0	-1.5403
2	3.3166	4.7287	-1.5560
3	2.9428	6.4612	-1.5599
4	2.7788	7.4153	-1.5616
5	2.6871	8.0260	-1.5625

Cases	$\alpha = 1.5$		
	$f''(-1)$	$g'(-1)$	$\theta'(-1)$
1	2.6648	2.6648	2.6648
2	2.3005	2.3005	2.3005
3	2.0183	2.0183	2.0183
4	1.8593	1.8593	1.8593
5	1.7587	1.7587	1.7587

Table 4 shows that the shear stress increases with the Reynolds number while slightly decreasing the heat transfer rate, for the case of contracting channel walls. However, the trend is reversed for the expanding walls. On the other hand, a remarkable rise in the couple stress is noted whether the walls are approaching or receding.

Table 4 Effect of the Reynolds number Re on $f''(-1), g'(-1)$ and $\theta'(-1)$ for

$C_1 = 4, C_2 = 0.8, C_3 = 0.4, M = 4$ and $Pr = 1.5$.

Re	$\alpha = -1.5$		
	$f''(-1)$	$g'(-1)$	$\theta'(-1)$
3.0	2.9879	8.4576	-1.5590
3.5	3.0032	8.9771	-1.5587
4.0	3.0199	9.4985	-1.5585
4.5	3.0378	10.0192	-1.5582
5.0	3.0567	10.5374	-1.5580

Re	$\alpha = -1.5$		
	$f''(-1)$	$g'(-1)$	$\theta'(-1)$
3.0	1.6564	10.1184	-0.4383
3.5	1.5667	11.7264	-0.4386
4.0	1.4844	13.5062	-0.4388
4.5	1.4125	15.4296	-0.4389
5.0	1.3527	17.4634	-0.4390

It is obvious from the Table 5 that the role of the external magnetic field is to enhance both the shear and couple stresses while lowering the heat transfer rate, for both the cases of α .

Table 5 Effect of the magnetic parameter M on $f''(-1), g'(-1)$ and $\theta'(-1)$ for

$C_1 = 4, C_2 = 0.8, C_3 = 0.4, Re = 1$ and $Pr = 1.5$

M	$\alpha = -1.5$		
	$f''(-1)$	$g'(-1)$	$\theta'(-1)$
0	2.7832	6.3829	-1.5619
25	3.6593	6.7894	-1.5511
50	4.3340	7.0627	-1.5437
75	4.8900	7.2619	-1.5382
100	5.3675	7.4151	-1.5339

M	$\alpha = 1.5$		
	$f''(-1)$	$g'(-1)$	$\theta'(-1)$
0	1.8141	5.4674	-0.4385
25	2.8971	6.0599	-0.4300
50	3.6818	6.4369	-0.4247
75	4.3067	6.7037	-0.4211
100	4.8321	6.9053	-0.4183

Table 6 predicts that the wall expansion ratio increases the shear and couple stresses as well as the heat transfer rate, when the walls are contracting. Again, a completely opposite trend is noted for the expanding walls.

It is clear from the Table 7 that the Prandtl number enhances the heat transfer rate only in case of contracting walls. It does not affect the other two physical quantities, due to the one way coupling of the governing equations (please see Eqs. (12)-(14)).

Physical model of the problem is shown in the Fig. 1, whereas the streamlines for the present problem are shown in the Fig. 2.

Table 6 Effect of the wall expansion ratio α on $f''(-1), g'(-1), \theta'(-1)$ for $C_1 = 4,$

$C_2 = 0.8, C_3 = 0.4, M = 4, Pr = 1.5$ and $Re = 1$

α	$f''(-1)$	$g'(-1)$	$\theta'(-1)$
-2.5	3.1683	6.6371	-2.1421
-1.5	2.9428	6.4612	-1.5599
0.0	2.5485	6.1076	-0.8755
1.5	2.0183	5.5850	-0.4368
2.5	1.4886	5.0734	-0.2608

Table 7 Effect of the Prandtl number Pr on $\theta'(-1)$ For $C_1 = 4, C_2 = 0.8, C_3 = 0.4, M = 4$ and

$Re = 1$

Pr	$\alpha = -1.5$	$\alpha = 1.5$
	$\theta'(-1)$	$\theta'(-1)$
0.1	-0.5462	-0.4955
0.5	-0.7662	-0.4781
0.9	-1.0421	-0.4611
1.3	-1.3742	-0.4448
1.7	-1.7575	-0.4289

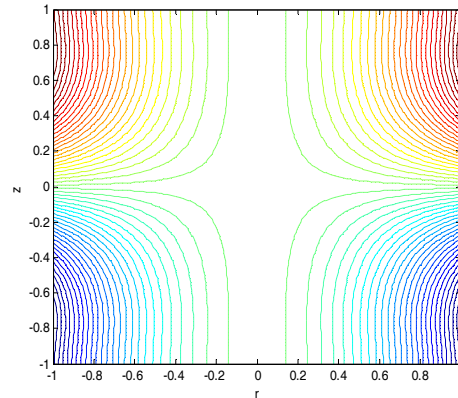


**Fig. 2. Contours of stream function for $C_1 = 4, C_2 = 0.8, C_3 = 0.4, Re = 5, Pr = 1.5,$
 $\alpha = 2.5, M = 4.$**

It is to mention that the position of viscous layer (the point $\eta = \eta_0$ for which $f(\eta) = 0$) lies in the middle of the channel, that is, in the plane $z = 0$, due to same amount of suction at the two walls.

However, it may shift towards either of the walls for the asymmetrical case, which may be a topic of a subsequent study. Moreover, the normal velocity takes its dimensionless value -1 at the lower wall, and acquires its maximum value 1 at the upper one, with a point of inflection lying at $\eta = 0$ (due to the symmetry of the problem) where it changes its concavity.

Figures (3-10) reflect the effect of the micropolar parameters on the velocity, microrotation and heat profiles. It is noted that, for both the cases of α , the micropolar parameters increase the magnitude of the normal velocity and the microrotation across the whole computational domain. The streamwise velocity is, however, raised only in the middle of the channel. Again, the micropolar parameters are not much influential for the thermal distribution.

For the case of expanding walls, the effect of the Reynolds number is similar to that of micropolar parameters (please see Figs. (11-18)). however, for the other case, we note two points: the Reynolds number is not much influential; and the way it affects the streamwise velocity and the microrotation, is changed.

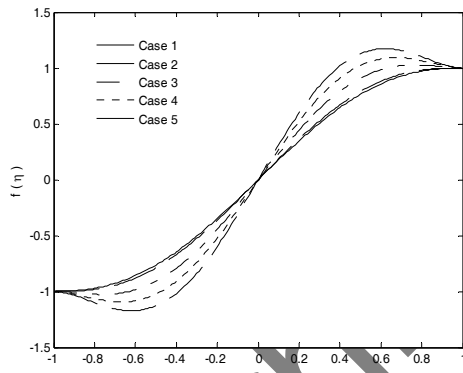


Fig. 3. Normal velocity profiles for $Re = 5, M = 4, Pr = 1.5, \alpha = 2.5$ and various cases of micropolar parameters.

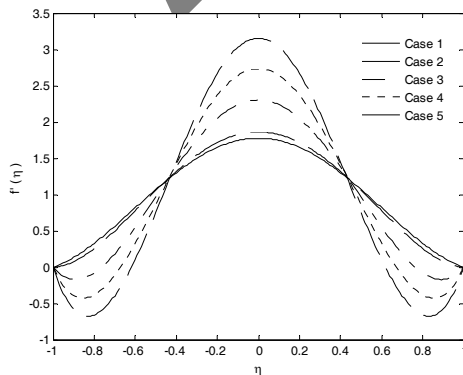


Fig. 4. Streamwise velocity profiles for $Re = 5, M = 4, Pr = 1.5, \alpha = 2.5$ and various cases of micropolar parameters.

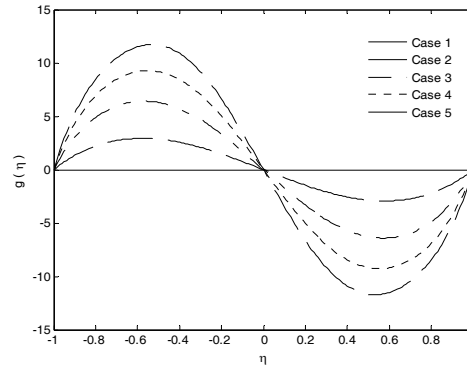


Fig. 5. Microrotation profiles for $Re = 5, M = 4, Pr = 1.5, \alpha = 2.5$ and various cases of micropolar parameters.

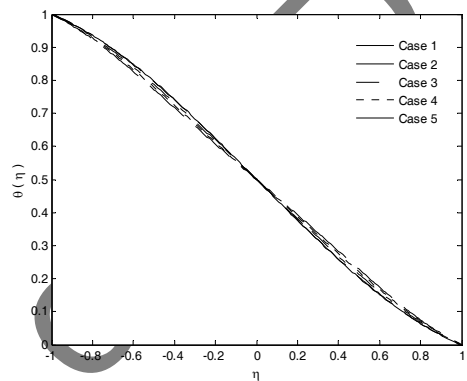


Fig. 6. Temperature profiles for $Re = 5, M = 4, Pr = 1.5, \alpha = 2.5$ and various cases of micropolar parameters.

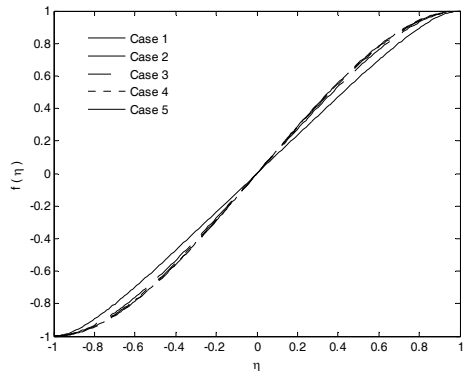


Fig. 7. Normal velocity profiles for $Re = 5, M = 4, Pr = 1.5, \alpha = -2.5$ and various cases of micropolar parameters.

It is clear from the Figs. (19-26) that, no matter the channel walls are expanding or contracting, the magnetic field exerts a drag like force (called the Lorentz force) on the fluid, which is responsible for reducing the normal velocity and the microrotation. The streamwise velocity, on the other hand, is raised in the small regions near the two channel walls. Hence the resistive force tends to drag the fluid towards the channel walls, which not only

results in increasing the shear stress at the wall but also causes greater spinning of the micro fluid particles hence, increases the couple stress as well (evident from Table 5).

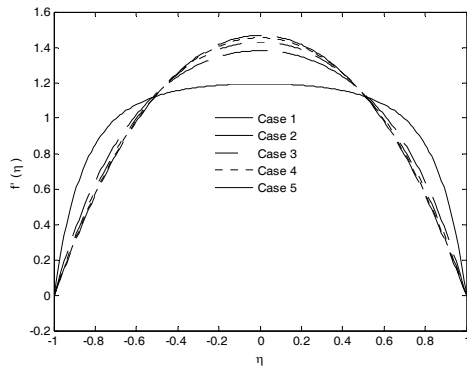


Fig. 8. Streamwise velocity profiles for $Re = 5, M = 4, Pr = 1.5, \alpha = -2.5$ and various cases of micropolar parameters.

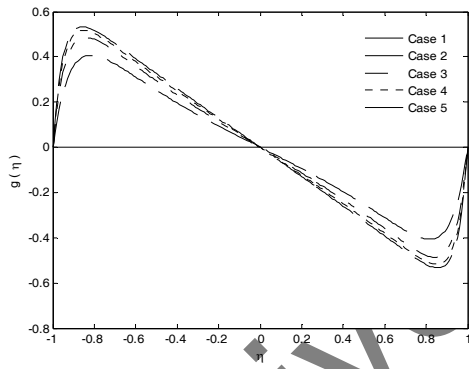


Fig. 9. Microrotation profiles for $Re = 5, M = 4, Pr = 1.5, \alpha = -2.5$ and various cases of micropolar parameters.

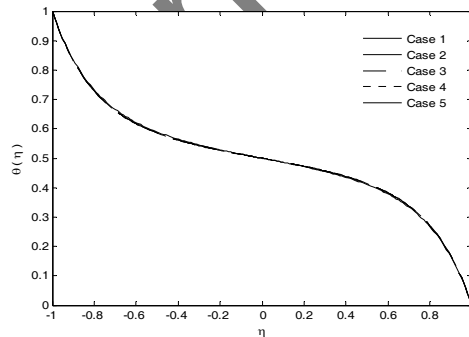


Fig. 10. Temperature profiles for $Re = 5, M = 4, Pr = 1.5, \alpha = -2.5$ and various cases of micropolar parameters.

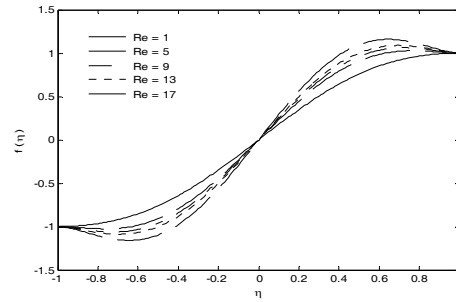


Fig. 11. Normal velocity profiles for $C_1 = 4, C_2 = 0.8, C_3 = 0.4, M = 4, Pr = 1.5, \alpha = 2.5$ and various Re .

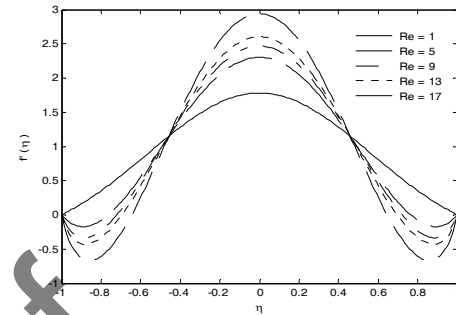


Fig. 12. Streamwise velocity profiles for $C_1 = 4, C_2 = 0.8, C_3 = 0.4, M = 4, Pr = 1.5, \alpha = 2.5$ and various Re .

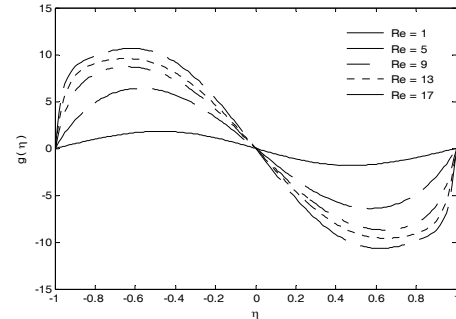


Fig. 13. Microrotation profiles for $C_1 = 4, C_2 = 0.8, C_3 = 0.4, M = 4, Pr = 1.5, \alpha = 2.5$ and various Re .

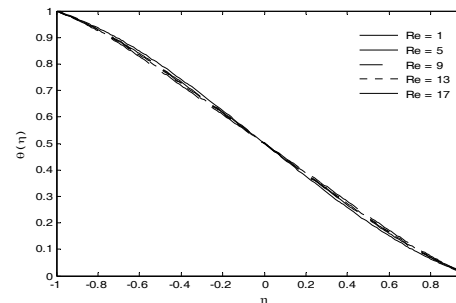


Fig. 14. Temperature profiles for $C_1 = 4, C_2 = 0.8, C_3 = 0.4, M = 4, Pr = 1.5, \alpha = 2.5$ and various Re .

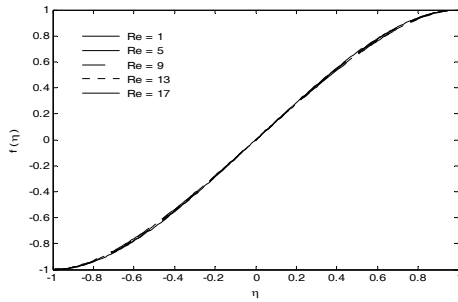


Fig. 15. Normal velocity profiles for $C_1 = 4, C_2 = 0.8, C_3 = 0.4, M = 4, Pr = 1.5, \alpha = -2.5$ and various Re .

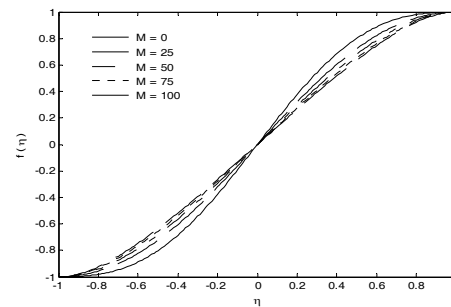


Fig. 19. Normal velocity profiles for $C_1 = 4, C_2 = 0.8, C_3 = 0.4, Pr = 1.5, Re = 2, \alpha = 2.5$ and various M .

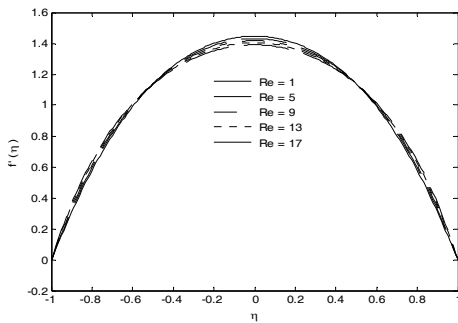


Fig. 16. Streamwise velocity profiles for $C_1 = 4, C_2 = 0.8, C_3 = 0.4, M = 4, Pr = 1.5, \alpha = -2.5$ and various Re .

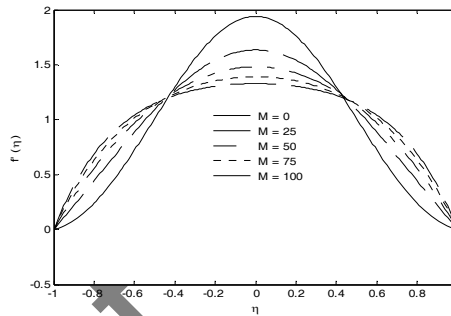


Fig. 20. Streamwise velocity profiles for $C_1 = 4, C_2 = 0.8, C_3 = 0.4, Pr = 1.5, Re = 2, \alpha = 2.5$ and various M .

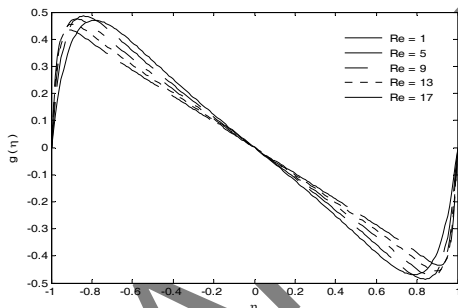


Fig. 17. Microrotation profiles for $C_1 = 4, C_2 = 0.8, C_3 = 0.4, M = 4, Pr = 1.5, \alpha = -2.5$ and various Re .

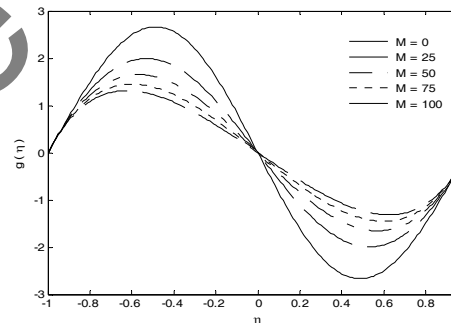


Fig. 21. Microrotation profiles for $C_1 = 4, C_2 = 0.8, C_3 = 0.4, Pr = 1.5, Re = 2, \alpha = 2.5$ and various M .

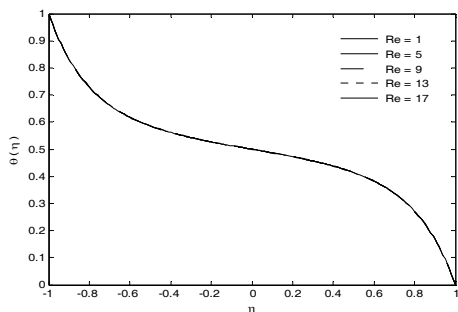


Fig. 18. Temperature profiles for $C_1 = 4, C_2 = 0.8, C_3 = 0.4, M = 4, Pr = 1.5, \alpha = -2.5$ and various Re .

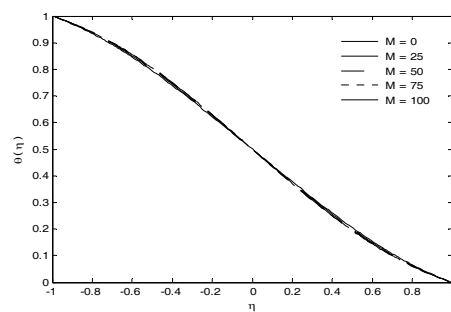


Fig. 22. Temperature profiles for $C_1 = 4, C_2 = 0.8, C_3 = 0.4, Pr = 1.5, Re = 2, \alpha = 2.5$ and various M .

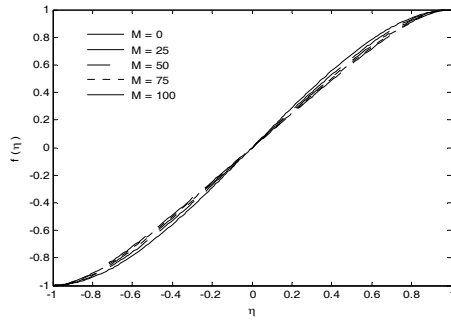


Fig. 23. Normal velocity profiles for $C_1 = 4, C_2 = 0.8, C_3 = 0.4, Pr = 1.5, Re = 2, \alpha = -2.5$ and various M .

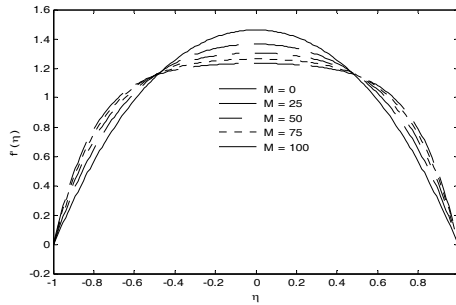


Fig. 24. Streamwise velocity profiles for $C_1 = 4, C_2 = 0.8, C_3 = 0.4, Pr = 1.5, Re = 2, \alpha = -2.5$ and various M .

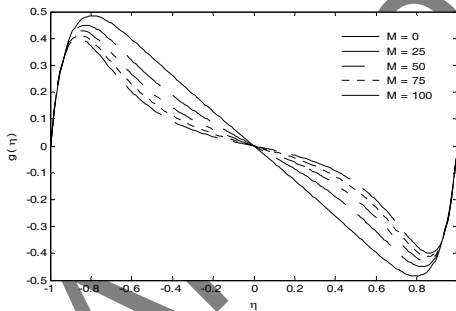


Fig. 25. Microrotation profiles for $C_1 = 4, C_2 = 0.8, C_3 = 0.4, Pr = 1.5, Re = 2, \alpha = -2.5$ and various M .

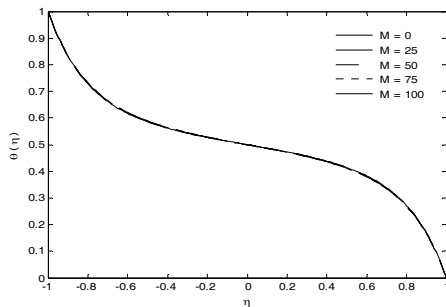


Fig. 26. Temperature profiles for $C_1 = 4, C_2 = 0.8, C_3 = 0.4, Pr = 1.5, Re = 2, \alpha = -2.5$ and various M .

As α varies from negative to positive, we note the rise in the magnitudes of the normal velocity and the microrotation across the whole domain. The temperature profile, however, tends to become an almost linear function of the dimensionless spatial variable η (please see Figs. (27-30)).

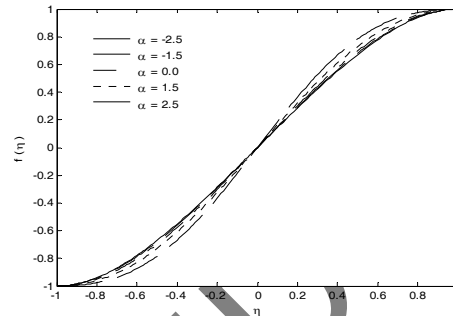


Fig. 27. Normal velocity profiles for $C_1 = 4, C_2 = 0.8, C_3 = 0.4, M = 4, Re = 2, Pr = 1.5$ and various α .

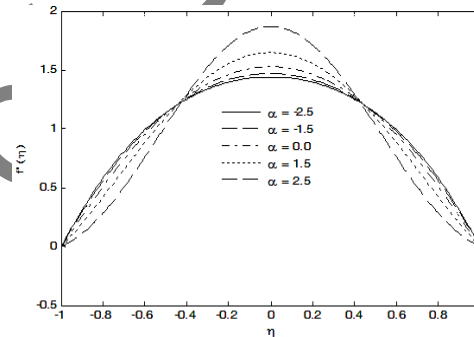


Fig. 28. Streamwise velocity profiles for $C_1 = 4, C_2 = 0.8, C_3 = 0.4, M = 4, Re = 2, Pr = 1.5$ and various α .

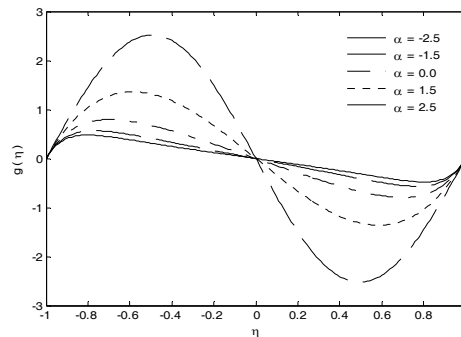


Fig. 29. Microrotation profiles for $C_1 = 4, C_2 = 0.8, C_3 = 0.4, M = 4, Re = 2, Pr = 1.5$ and various α .

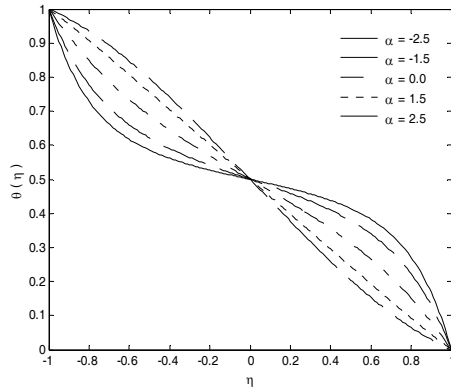


Fig. 30. Temperature profiles for
 $C_1 = 4, C_2 = 0.8, C_3 = 0.4, M = 4,$
 $Re = 2, Pr = 1.5$ and various α .

Figures (31-32) show that, in the case of contracting walls, the Prandtl number tends to lower the thermal distribution in the lower half of the channel whereas an opposite effect is noted in the upper half. The trend is however reversed for the case of expanding walls.

Compared with the work of Aski *et al.* 2014, we have noticed a qualitative change in the way in which the micropolar parameters and the Reynolds number affect the streamwise velocity profiles in case of expanding walls. Both the parameters tend to lower the velocity distribution near both the walls, predicting a negative velocity component in these regions. Thus, the parabolic nature of the profile for the Newtonian fluid at low Reynolds number is changed. No such change was noticed in the work of Aski *et al.* 2014, where the channels were stationary. We therefore conclude that this particular influence of the micropolar parameters and the Reynolds number is due to the expanding channel walls. Moreover, we notice a non uniform way in which the Reynolds number affects the microrotation profiles for the case of approaching walls. It decreases the magnitude of the microrotation everywhere except for the small regions near the two walls where the trend is opposite, which is again contrary to the results reported by Aski *et al.* 2014.

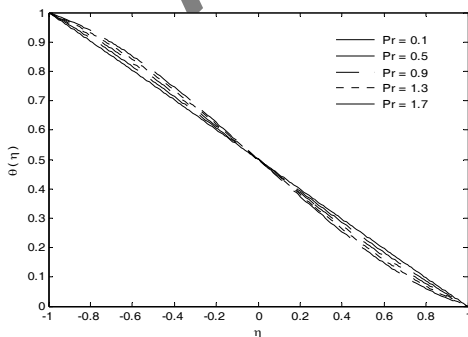


Fig. 31. Temperature profiles
for $C_1 = 4, C_2 = 0.8, C_3 = 0.4, M = 4,$
 $Re = 2, \alpha = 2.5$ and various Pr .

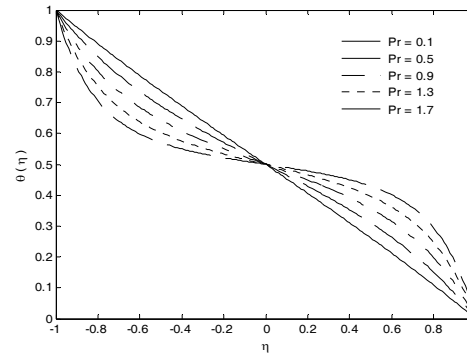


Fig. 32. Temperature profiles for
 $C_1 = 4, C_2 = 0.8, C_3 = 0.4, M = 4,$
 $Re = 2, \alpha = -2.5$ and various Pr .

5. CONCLUSUONS

The characteristics of laminar, incompressible, viscous and unsteady flow of an electrically conducting micropolar fluid in a porous channel with expanding or contracting walls under the action of an applied magnetic field are explored numerically.

It has been observed that the micropolar structure of the fluid is responsible for reducing the shear stress while increasing the couple stress and the heat transfer rate at the channel walls, whether the walls are expanding or contracting. The shear stress increases with the Reynolds number while slightly decreasing the heat transfer rate, only for the case of contracting channel walls. The external magnetic field always enhances both the shear and couple stresses while lowering the heat transfer rate. The wall expansion ratio increases or decreases the three physical quantities according to the case of contracting or expanding walls, whereas the Prandtl number enhances the heat transfer rate only in case of contracting walls.

The micropolar parameters increase the magnitudes of the normal velocity and the microrotation across the channel, for the both wall conditions. For approaching walls, the Reynolds number decreases the magnitude of the microrotation everywhere except for the small regions near the two walls where the trend is opposite. No matter the channel walls are expanding or contracting, the magnetic field reduces the normal velocity and the microrotation. In case of expanding walls, the micropolar parameters and the Reynolds number tend to lower the velocity distribution near both the channel walls, predicting a negative velocity component in these regions. For contracting walls, the Prandtl number tends to lower the thermal distribution in the lower half of the channel whereas an opposite effect is noted in the upper half. The trend is however reversed for the case of expanding walls.

ACKNOWLEDGEMENTS

The authors are extremely grateful to the Higher

Education Commission of Pakistan for the financial support to carry out this research. The authors are also grateful to the learned reviewers for their comments to improve the quality of this paper.

REFERENCES

- Ali, K. and M. Ashraf (2014). Numerical simulation of the micropolar fluid flow and heat transfer in a channel with a shrinking and a stationary wall. *Journal of Theoretical and Applied Mechanics* 52, 557-569.
- Ali, K., F. M. Iqbal, Z. M. Akbar and M. Ashraf (2014). Numerical simulation of unsteady water-based nanofluid flow and heat transfer between two orthogonally moving porous coaxial disks. *Journal of Theoretical and Applied Mechanics* 52, 1033-1046.
- Ali, K., M. Ashraf, and N. Jameel (2014). Numerical simulation of magnetohydrodynamic micropolar fluid flow and heat transfer in a channel with shrinking walls. *Canadian Journal of Physics* 92(9), 987-996.
- Ali, K., Z. M. Akbar, F. M. Iqbal and M. Ashraf (2014). Numerical simulation of heat and mass transfer in unsteady nanofluid between two orthogonally moving porous coaxial disks. *AIP Advances*. 4.
- Ashmawy, E. A. (2014). Fully developed natural convective micropolar fluid flow in a vertical channel with slip. *Journal of the Egyptian Mathematical Society*.
- Govardhan, K. and N. Kishan (2011). Unsteady MHD boundary layer flow of an incompressible micropolar fluid over a stretching sheet. *Journal of Applied Fluid Mechanics*. 5(3), 23-28.
- Khoshab, M. and A. A. Dehghan (2011). Numerical simulation of buoyancy-induced micropolar fluid flow between two concentric isothermal spheres. *Journal of Applied Fluid Mechanics* 4(2), 51-59.
- Majdalani, J. and C. Zhou (2003). Moderate-to-large injection and suction driven channel flows with expanding or contracting walls. *Zeitschrift für Angewandte Mathematik and Mechanik* 83(3), 181-196.
- Umavathi, J. C. (2011). Mixed convection of micropolar fluid in a vertical double-passive channel. *International Journal of Engineering, Science and Technology* 3(8), 197-209.
- Xin-Hue, SI., Z. Lian-Cun, Z. Xin-Xin and Y. Chao (2010). Analytic solution to the micropolar fluid flow through a semi-porous channel with an expanding or contracting wall. *Applied Mathematics and Mechanics -English Edition* 31(9) 1073-1080.
- Xin-Hue, SI., Z. Lian-Cun, Z. Xin-Xin, SI. Xin-Yi and Y. Jian-Hong (2011). Flow of a viscoelastic fluid through a porous channel with expanding or contracting walls. *Chin. Phys. Lett.* 28(4), 044702.
- Xinhui, S., Z. Liancun, Z. Xinxin, S. Xinyi, and L. Min (2012). Asymmetric viscoelastic flow through a porous channel with expanding or contracting walls: a model for transport of biological fluids through vessels. *Computer Methods in Biomechanics and Biomedical Engineering* 17(6), 623-31.

Archive of SID

SID



سرویس های ویژه



سرویس ترجمه تخصصی



کارگاه های آموزشی



بلاگ مرکز اطلاعات علمی



عضویت در خبرنامه

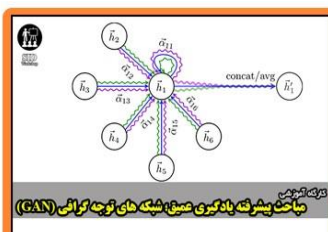


فیلم های آموزشی

کارگاه های آموزشی مرکز اطلاعات علمی جهاد دانشگاهی



کارگاه آنلاین آشنایی با پایگاه های اطلاعات علمی بین المللی و ترند های جستجو



مباحث پیشرفته یادگیری عمیق؛ شبکه های توجه گرافی (Graph Attention Networks)



کارگاه آنلاین مقاله نویسی IEEE و ISI ویژه فنی و مهندسی